Effect of basalt fiber inclusion on the mechanical properties and microstructure of cement-solidified kaolinite

D. Wang, H. Wang, S. Larsson, M. Benzerzour, W. Maherzi, Mouhamadou Amar

Effect of basalt fiber inclusion on the mechanical properties and microstructure of cement-solidified kaolinite

Dongxing WANG[a,c], Hongwei WANG[a,b,*], Stefan LARSSON[c], Mahfoud BENZERZOUR[b], Walid MAHERZI[b], Mouhamadou AMAR[b]

a Key Laboratory of Geotechnical and Structural Engineering Safety of Hubei Province, School of Civil Engineering, Wuhan University, 430072 Wuhan, China.

b Department of Civil Engineering and Environmental, IMT Lille Douai, EA 4515 - LGCgE, University of Lille, F-59000 Lille, France.

c Department of Civil and Architectural Engineering, School of Architecture and the Built Environment, KTH Royal Institute of Technology SE-10044, Stockholm, Sweden.

Abstract: **The polypropylene fibers, which are currently attracting enormous attention in various geotechnical applications, carry a risk of aging under an integrated effect of heat, oxygen, light and other environmental factors, causing potentially infrastructure failure. An eco-friendly and biologically inactive material – basalt fiber, which has excellent natural resistance to aging and can eliminate aging-associated disasters, deserves more attention in geotechnical field. However, quite few studies are available on the beneficial reuse of basalt fibers to improve the engineering performance of soils. Therefore, this study aims to incorporate the sustainable basalt fiber and clarify how its inclusion** impacts the mechanical properties and microstructure of cemented kaolinite. The experimental programs are comprised of three types of tests, i.e. two to examine the compressive strength and triaxial shear behavior and one to evaluate the microstructure properties. **The results** indicate that the basalt fiber reinforcement plays an essential role in enhancing the compressive strength and peak deviatoric stress of cemented and uncemented kaolinite. **The inclusion of basalt fibers improves the ductility and weakens the brittleness of cemented kaolinite. The compressive strength increases with basalt fiber content and curing time, and reaches the peak at the fiber content of 0.2 %, followed by a reduction due to the formation of weak zone at higher fiber content.** The peak deviatoric stress is elevated until reaching the maximum at the basalt fiber content of 0.4 %, after which further addition of basalt fiber tends to reduce its reinforcing effect. The peak deviatoric stress increases as the basalt fiber length is shortened and the confining pressure is raised. **The strength**

gain of cement-basalt fiber inclusion is much more than the sum of strength increase induced by them individually. The combination of basalt fiber and cement has the virtues of both cement-stabilized and basalt fiber-reinforced kaolinite. The SEM analysis reveals that the mechanical interaction in the form of interface bonding and friction between kaolinite particle, cement hydration product and basalt fiber is the dominant mechanism controlling the reinforcement-cementation **benefits. The bridging effect (reinforcement) of basalt fibers and binding effect (cementation) of hydration products make a major contribution to the formation of stable and interconnected microstructure,** which results in an evident improvement in the mechanical behaviour of cemented kaolinite. **The combination of basalt fiber and cement stabilization would be an innovative and effective method for geotechnical engineering works such as soft ground improvement**.

Keywords: Basalt fiber; cemented kaolinite; compressive strength; peak deviatoric stress; micro-mechanisms

1 Introduction

In the east-coastal area of China, soft clay is widely distributed and commonly encountered, which is the composition of clayey sedimentary or river flushing [1]. Over recent years, along with boost economic development and rapid population growth, a huge amount of construction engineering projects such as highway, land reclamation, airport, offshore wind power and sea-crossing bridge have to be built on soft clay grounds. However, the engineering performance of soft clay is worrying and

troublesome, principally because of its high water content, high compressibility, low permeability and low bearing capacity. Fortunately, the detrimental effect of soft clay can be effectively overcome by cement/lime solidification process, which is a cost-competitive and efficient route. Hence, cement/lime stabilization technology is becoming more and more popular for soft clay improvement all over the world. It is well known that the cementitious materials such as cement, lime, Class F fly ash, Class C fly ash, lime kiln dust and fiber as reported in [2-11] have been incorporated in soil stabilization.

Currently, the fiber as a promising reinforcing material is commonly employed to reinforce cement/lime-treated soft clay in civil engineering practices. Many studies through a number of triaxial compression (TC), unconfined compressive strength (UCS), bearing capacity and direct shear tests have already been conducted to elucidate the effect of fiber reinforcement on cement/lime-treated soft clay. Wang et al. [11] investigated the coupling effect of wheat straw fiber and lime, and even a small amount of wheat straw fibers could improve their intensity of the strain-softening behavior associated with lime stabilization. Tang et al. [12] found that the randomly distributed polypropylene fibers significantly improve the tensile behavior and peak strength of soils and reduce soil cracking. Ammar et al. [13] showed that the interface shear strength parameters of natural hemp fiber-clay are largely affected by the testing mechanisms and drainage conditions based on the interface direct shear and single fiber pullout tests. Wang et al. [14] developed a useful modeling approach to predict the pre-failure and failure behavior of fiber-reinforced clay subjected to TC tests, and

the predicted behavior was proved to have a good agreement with the experimental response. The above-stated researches have shown that the fiber can be considered as a good earth reinforcement material, which induces greater strength, roughness and ductility and smaller post-peak strength loss, as compared to soil alone. However, the fibers used in these studies are mostly polypropylene fibers, and only a few works [15,16] **focusing principally on the dynamic properties** have ever attempted to introduce basalt fiber in soil reinforcement. **Until now, the triaxial and uniaxial compression behavior of basalt fiber-reinforced cemented soil and microstructural interaction between basalt fiber and cemented soil matrix** which deserve to be further investigated are rarely reported.

In recent years, the basalt fiber owning to its sustainability and environmentally friendly property has already been proved to be a good substitute for other fiber materials in geotechnical engineering. As a green and environmentally friendly fiber that attracts very little attention until now, it uses natural basalt ore as raw material and the major ingredients are SiO_2, Al_2O_3, FeO and Fe_2O_3. Especially, it is a typical silicate fiber, which has a good natural compatibility (non-hazardous, biologically inactive) with cement composite, excellent mechanical property, high temperature and acid and alkali resistance. The mechanical property of basalt fiber is largely higher than that of polypropylene fiber, but its price is only 1/10 of conventional carbon fiber [17,18]. It has been widely used as the insulation, sound absorption and heat-resistant materials to modify concrete [19-23]. However, the above literature reveals that the application of basalt fiber to the soil reinforcement is indeed rarely reported until now

and the relevant studies are really lacking in the mechanical and microstructural properties of basalt fiber-reinforced soils. As a result, more attentions should be given on the performance and mechanism of basalt fiber to reinforce soft clay, especially in terms of **basalt fiber** reinforcement in cemented clay.

Therefore, the objective of this study is to **better understand** the effect of basalt fiber inclusion on the mechanical behavior of cemented kaolinite and identify the corresponding microstructural mechanisms. In order to **clearly** investigate the influence of several factors including basalt fiber content, fiber length, curing time and confining pressure σ_3, a series of UCS and consolidated-undrained (CU) TC tests are carried out on cemented kaolinite. The interfacial interaction between basalt fibers, cement hydration products and kaolinite particles and **the relevant** microstructure of fiber-reinforced cemented kaolinite are deeply discussed by conducting scanning electron microscopy (SEM) tests, to obtain a preliminary knowledge of the intrinsic mechanisms of basalt fiber inclusion. The final purpose of this study is to propose a novel combination of basalt fiber with cement, which can provide some reference for soft ground improvement.

2 Materials and methods

2.1 Materials

Kaolinite (abbreviated to K) with grey color was obtained from a kaolinite manufacturer Co. LTD in Yidu city in China, since it is easily obtained in practice. As shown in Table 1, the basic physical characteristics of tested kaolinite were determined in laboratory according to *the standard test methods of soils for highway*

133 *engineering defined by JTG E40-2007* [24]. The initial water content of kaolinite is
134 0.17 %. The specific gravity is 2.75 determined by the pycnometer test. The liquid
135 limit and plastic limit are, respectively, 31.0 % and 20.1 %, measured by the
136 liquid-plastic limit combined test method. Thus, the plasticity index value of this
137 kaolinite material is 10.9 %, which shows a low compressibility. The modified Proctor
138 compaction test provides an optimum water content of 22.4 % and maximum dry
139 density of 1.62 g/cm^3 for the tested kaolinite.
140 The cement used in this study is P.O 42.5 ordinary Portland cement (P), and its
141 chemical compositions are listed in Table 2. The basalt fibers (B), as presented in Fig.
142 1, have the length of monofilament of 3 mm, 7 mm and 11 mm. The technical
143 specifications of the chosen basalt fibers are summarized in Table 3. The basalt fiber
144 has a density of 2.63 g/cm^3, which is similar to the maximum dry density of kaolinite.
145 The parameters of monofilament are 7-15 μm in diameter, 1050 °C in melting point,
146 tensile strength of 3000-4800 MPa and modulus of elasticity of 91-110 GPa. The
147 above-mentioned data indicate that the basalt fiber has excellent mechanical property,
148 corrosion resistance and acid and alkali resistance.

149 ## 2.2 Sample preparation and test methods

150 ### 2.2.1 Unconfined compressive strength test

151 The mixture design formulations for investigating the effect of basalt fiber on
152 cemented kaolinite are reported in Table 4, where the abbreviation of KxPyB-z
153 represents the kaolinite samples solidified with x % cement and y % basalt fiber with
154 length of z mm. All the tested samples were prepared under the conditions of optimum

moisture content and maximum dry density determined by the modified Proctor compaction tests. To control the economic cost and avoid the fiber agglomeration during mixing, the used basalt fiber contents were 0, 0.1 %, 0.2 %, 0.3 % and 0.4 % for UCS tests, calculated on the dry mass of kaolinite, while the cement content was fixed at 6 % of dry kaolinite weight. **It is noteworthy that the basalt fiber contents are chosen based on previous studies [12,17,25] and 6% cement is fixed since it was proved as an economic and reasonable amount to improve the engineering property of soil according to [26]**. First, the distilled water and kaolinite were mixed by a mechanical mixer until the optimum water content of 22.4 % was reached, and afterwards stored in an airtight container for 24 h to achieve an internal uniform moisture distribution. Second, the basalt fibers and cement were simultaneously added in the prepared moist kaolinites and mixed together for 10 mins by a laboratory mechanical mixer, and a visual examination was performed to ensure the homogeneity of mixture. Finally, the prepared mixture was put into a cylindrical mould of 50 mm in diameter and 50 mm in height, and later compacted and demolded through a hydraulic jack. The demolded cylindrical samples were immediately sealed with plastic film, and cured at constant temperature of 20 ± 2 °C and relative humidity of 95 ± 2 % for 3 d, 7 d, 14 d, and 28 d. The UCS tests were performed with a universal testing machine, and the vertical loading was applied to the sample at a constant displacement rate of 1 mm/min until failure. Three samples were tested for each mixture and the average value was calculated to determine the compressive strength. Note that all the tests were extended to the basalt fiber-reinforced kaolinite (Group 1) as reference, to make

177 a comparison between basalt fiber-reinforced uncemented kaolinite (BFUK) and
178 basalt fiber-reinforced cemented kaolinite (BFCK) (Group 2).

179 **2.2.2 Undrained triaxial compression test**

180 A similar approach was employed in triaxial tests to prepare samples in the cylindrical
181 moulds with 39.1 mm in diameter and 80 mm in height **according to *the standard***
182 ***test methods of soils for highway engineering defined by JTG E40-2007*** **[24]**. As
183 shown in Table 4, the designed samples for triaxial tests are kaolinite samples
184 solidified with constant cement content of 6 % and different amounts of basalt fibers
185 with different lengths. Thereafter, Group 3 was developed to investigate the effect of
186 basalt fiber inclusion on the triaxial shear behavior of cemented kaolinite. The basalt
187 fiber contents chosen in Group 3 are 0, 0.1 %, 0.2 %, 0.3 %, 0.4 % and 0.5 % by
188 weight of dry kaolinite powder, and the basalt fiber length is a constant of 11 mm in
189 this case. To investigate the impact of basalt fiber length, Group 4 was designed given
190 that the fiber lengths are 3 mm, 7 mm and 11 mm and the basalt fiber contents are
191 settled at 0.2 % by weight of dry kaolinite. By using a static compaction method, each
192 sample for triaxial tests was compacted in three layers to ensure a uniform compaction
193 degree. Once the sample preparation was completed, the samples were sealed with
194 hermetical plastic film and cured at room temperature of 20 ± 2 °C and relative
195 humidity of 95 ± 2% for 7 d. After that, the consolidated undrained (CU) triaxial tests
196 were carried out according to Chinese standard JTG E40-2007 [24], and each of the
197 samples was tested at three different confining pressures of 50 kPa, 100 kPa and 200
198 kPa at constant vertical strain rate of 0.1 mm/min. During the loading process, the

199 deviatoric stress $q = \sigma_1-\sigma_3$ was recorded as a function of axial strain ε until the
200 post-failure regime, and the maximum ε that was permitted to occur in triaxial tests
201 was 5 %. Especially, the whole shearing process was automatically controlled by a
202 specialized computer to realize a real-time acquisition of test data.

203 **2.2.3 SEM test for morphological analysis**

204 The representative specimens after unconfined compression tests were chosen for the
205 detailed microstructural characterization of cement-fiber solidified kaolinites by using
206 scanning electron microscopy. The selected specimens were dried in an oven at 40 ℃
207 until they attained constant weight, and then the blocks of a size of about 1 cm^3 were
208 prepared. The scanning electron microscopy specimens should be first gold-coated by
209 a sputtering technique to make them conductive and avoid charging effect. Finally, the
210 associated internal changes in the microstructure of cement-treated specimens owning
211 to the basalt fiber inclusion were identified through SEM analysis on FEI Quanta 200
212 machine.

213 # 3 Results and Discussion

214 ## 3.1 Unconfined compressive strength behavior

215 **3.1.1 Stress-strain relationship**

216 The stress-strain curves of BFUK and BFCK defined by UCS tests are shown in Fig.
217 2, where all the samples were prepared at varying basalt fiber contents and cured for
218 28 d. It can be seen from Fig. 2 (a) that for BFUK without fiber (K0B), the vertical
219 stress σ_1 increases until its peak of 0.21 MPa corresponding to the failure strain ε_f of
220 3.2 % as the axial strain ε extends, followed by a sharp decrease in stress. The ε_f

values of BFCK with 0.1 %, 0.2 %, 0.3 % and 0.4 % basalt fibers are respectively 3.2 %, 3.6 %, 3.6 % and 4.3 %, while the corresponding peak stress is 0.20 MPa, 0.25 MPa, 0.24 MPa and 0.20 MPa. Compared with K0B, it is evident that the peak stress decreases slightly at the basalt fiber content of 0.1 % (K0.1B-3) and 0.4 % (K0.4B-3), and then goes up if the basalt fiber content changes to 0.2 % (K0.2B-3) and 0.3 % (K0.3B-3).

Fig. 2 (b) describes the variation of stress-strain curves of BFCK samples with various basalt fiber contents at 28 d. Upon comparison with Fig. 2 (a), it can be seen that the peak axial stress σ significantly increases owing to the addition of 6 % cement and the maximum peak stress appears for BFCK sample with 0.2 % of basalt fiber (K6P0.2B-3). The σ is initially elevated with an increase in ε until the peak stress is reached, and then the σ decreases sharply as the ε continues to rise. Owing to the effect of cement stabilization, the ε_f of BFCK with 0.1 %, 0.2 %, 0.3 % and 0.4 % basalt fibers are 3.1 %, 3.4 %, 3.5 % and 3.3 %, respectively, and the peak stress is correspondingly 5.49 MPa, 6.56 MPa, 5.72 MPa and 5.48 MPa.

Especially, both the BFUK and BFCK samples reinforced with basalt fiber exhibit a more ductile behavior since the failure strain ε_f is more or less raised due to the effect of fiber inclusion. This finding accords well with the previous studies reported in [11,12,15]. Furthermore, the post-peak stress level of BFCK samples is intensified owing to the addition of basalt fiber under the same ε. It is undoubted that one of the main advantages related to the reinforcement effect of basalt fiber when applied to kaolinite is the improvement in material ductility.

Especially, from the typical stress-strain curves such as BFUK (K0.2B-3) and BFCK (K6P0.2B-3), it can be concluded that the curves can be divided into four stages: (i) initial compaction stage: the fine particles rearrange and orientate themselves under very low vertical loading, diminishing the interparticle pore volume; (ii) elastic deformation stage: the σ approximately increases linearly when the ε increases; (iii) plastic deformation stage: the σ has a relatively slow growing trend with increasing ε before the σ reaches its peak; (iv) post-failure stage: once the σ exceeds the peak strength, it starts to decreases sharply as the ε slightly increases.

3.1.2 Unconfined compressive strength

Fig. 3 (a) and (b) shows respectively the variation of UCS of BFUK and BFCK samples with varying basalt fiber contents. For BFUK samples in Fig. 3(a), the maximal UCS occurs at the curing time of 28 d, where the UCS decreases a little from 0.21 MPa (K0B) to 0.2 MPa (K0.1B), and then rises to 0.262 MPa with the increase of basalt fiber content from 0 to 0.1 % and 0.2 %. However, further increase in basalt fiber content from 0.2 % to 0.3 % and 0.4 % produces a downward trend of UCS, being reduced correspondingly from 0.262 MPa to 0.256 MPa and 0.202 MPa. Hence, it could be deemed that the suitable content of embedded basalt fiber for reinforcing BFUK samples is around 0.2 %, where the highest UCS is reached. For BFUK samples with varying basalt fiber contents, their UCS tends to increase with curing time from 3 d to 28 d, which might be due to the water evaporation from the surface and inside of samples. The reduction in the water content of samples induces an observable augmentation in the UCS with increasing curing time.

As shown in Fig. 3 (b), a slight decrease in UCS because of the inclusion of 0.1 % basalt fiber (K6P0.1B) is observed as compared to the sample without basalt fiber (K6P0B), independent of curing time from 3 d to 28 d. The 28-day UCS of samples increases respectively by -1.90 %, 22.92 %, 10.11 % and 3.67 % with basalt fiber content from 0.1 % to 0.4 %, as compared to cemented kaolinite without basalt fiber (K6P0B). These analyses indicate that the suitable content of basalt fiber for 6 % cement solidified samples is around 0.2 % according to the change of UCS. At the basalt fiber content of 0.2 %, the UCS of fiber-reinforced cemented kaolinite at 7 d, 14 d and 28 d is respectively 5.20 MPa, 6.26 MPa and 6.55 MPa, increasing by 25.00 %, 50.48 % and 57.45 % as compared with the corresponding sample at 3 d (4.16 MPa).

In addition, the UCS and strength increase of basalt fiber plus cement solidified samples in Fig. 3 (b) is far more significant than that generated singly by the basalt fiber inclusion in Fig. 3 (a). Under the condition of 0, 0.1 %, 0.2 %, 0.3 % and 0.4 % basalt fiber inclusion, the 28-day strength of BFCK increases correspondingly by 25.87, 26.48, 24.02, 21.38 and 26.09 times as compared with the corresponding BFUK samples. Especially, a combination of 0.2 % basalt fiber and 6% cement for 28-day kaolinite sample K6P0.2B produces a strength of 6.55 MPa, which is greater than both the strength brought by 0.2 % basalt fiber (i.e. sample K0.2B, 0.262 MPa) and the strength generated by 6 % cement (i.e. sample K6P0B, 5.64 MPa).

From the obtained results, it can be seen that the basalt fiber content and curing time play an observable role in the UCS levels. The cementation effect from the cement

hydration is much more important than the reinforcing effect of basalt fiber for the UCS amelioration of kaolinite, which has been reported by Wang et al. [11]. The strength gain analysis indicates that the combined effect of basalt fiber and cement within soil matrix (i.e. interfacial mechanical interaction) is not a simple summation of their individual contribution, but is in fact a complex coupled effect on the strength improvement. This conclusion coincides well with the result obtained by Wang et al. [11].

3.2 Triaxial shear behavior

3.2.1 Deviatoric stress versus axial strain

The typical relationships of deviatoric stress q versus axial strain ε obtained by triaxial compression (TC) tests are shown in Fig. 4, where BFCK sample exhibits an obvious strain-softening behavior. Fig. 4 (a) presents the q versus ε curves of BFCK samples at varying basalt fiber contents and constant confining pressure σ_3 of 100 kPa. The q-ε relationships of BFCK are discussed merely for σ_3 of 100 kPa due to the similarity of the q-ε behavior between different σ_3 levels. It appears that the basalt fiber inclusion contributes to an improvement in the peak deviatoric stress q_p of cement-treated kaolinite samples. The magnitude of this contribution, which varies depending on the basalt fiber content, tends to increase with increasing basalt fiber content from 0.1 % to 0.4 % and afterwards decreases slightly in case of further elevating the fiber content to 0.5 %.

The q-ε curves obtained from TC tests are given in Fig. 4 (b) for BFCK samples with varying basalt fiber lengths and at σ_3 of 100 kPa. It can be seen from Fig. 4 (b) that the q_p of BFCK samples with 0.2 % basalt fiber significantly increases with basalt fiber length reduced from 11 mm to 3 mm, and the maximum q_p occurs at the fiber

311 length of 3 mm. As reported in Fig. 4 (c), three different levels of σ_3 including 50 kPa,
312 100 kPa and 200 kPa were employed to evaluate the q-ε curves of samples
313 K6P0.2B-11 and K6P0B. As expected, the results demonstrate that the q_p of BFCK
314 can be greatly improved as σ_3 goes up from 50 kPa to 200 kPa.
315 Therefore, the above-mentioned results reveal that these factors including basalt fiber
316 content, basalt fiber length and confining pressure level could have an important
317 impact on the q-ε behavior of fiber-cement reinforced sample. The optimal basalt
318 fiber content to ameliorate the q-ε behavior of BFCK can be approximately
319 considered as 0.4 %, which is evidently different from the optimal basalt fiber content
320 estimated by UCS tests. Compared to long basalt fibers, shorter discrete fiber mixed
321 uniformly within the soil mass can increase the number of fibers in a unit volume of
322 soil mass, and the acquired reinforcement benefit of basalt fiber to UCS is therefore
323 more pronounced. The lateral deformation of tested samples could be further
324 prevented at higher confining pressure, which enhances to a certain extent the UCS
325 levels.

326 **3.2.2 Variation of peak deviatoric stress**

327 It is obvious to know from Fig. 4 that BFCK samples exhibit strain-softening behavior.
328 Figures 5-7 show the variation of q_p and peak stress ratio R_f of BFCK with basalt fiber
329 content, basalt fiber length and confining pressure. The peak stress ratio R_f is defined
330 as the ratio of peak deviatoric stress q_{pr} of reinforced samples to that of unreinforced
331 samples (without fiber) q_{p0} [27].

332 $$R_f = \frac{q_{pr}}{q_{p0}}$$

333 Fig. 5 shows the effect of varying basalt fiber contents (0, 0.1 %, 0.2 %, 0.3 %, 0.4 %
334 and 0.5 %) on the q_p and R_f of BFCK samples. For instance, at the σ_3 of 100 kPa, the

q of cemented kaolinite sample without basalt fiber (K6P0B) is 2.11 MPa, while the addition of 0.1 %, 0.2 %, 0.3 %, 0.4 % and 0.5 % basalt fiber results in an increase of q to 2.64 MPa (K6P0.1B), 2.82 MPa (K6P0.2B), 3.36 MPa (K6P0.3B), 3.62 MPa (K6P0.4B) and 3.40 MPa (K6P0.5B). The R_f correspondingly increases from 1.0 (K6P0B) to 1.25 (K6P0.1B), 1.33 (K6P0.2B), 1.59 (K6P0.3B), 1.71 (K6P0.4B) and 1.61 (K6P0.5B).

The results reveal that the addition of basalt fiber as reinforcing materials provides an approach to enhance the q_p of cemented kaolinite, and the percentage of basalt fiber plays a significant role in improving the q_p of BFCK. Especially, q_p of cemented kaolinite reaches the optimum level at 0.4 % of basalt fiber when compared with other basalt fiber contents, and higher or lower amount of basalt fiber would bring about a decrease in the q_p of basalt fiber-cement solidified kaolinite samples. It is interesting to note that a similar trend can be observed for the change of R_f ratio with basalt fiber content. R_f tends to increase continuously with basalt fiber content, and the maximum ratio occurs also at 0.4 % of basalt fiber, being independent of σ_3 levels.

Fig. 6 shows the effect of varying basalt fiber lengths (0, 3 mm, 7 mm and 11 mm) on the q_p and R_f of BFCK. For a specific percentage of 0.2, it can be observed that the introduction of basalt fiber with length of 3 mm, 7 mm and 11 mm improves greatly the q_p of cemented kaolinite compared to the control sample - cemented kaolinite without basalt fiber (i.e. K6P0B, 2.59 MPa). The q_p value reaches up to 4.52 MPa, 3.65 MPa and 3.40 MPa after adding 0.2 % basalt fiber with length of 3 mm, 7 mm and 11 mm respectively, while the corresponding R_f changes from 1.0 to 1.45, 1.33 and 1.31. Similar to the strength variation with basalt fiber content, the q_p and R_f has a rising trend with fiber length until their individual peak, followed by an observable reduction as a result of further prolongation of fiber length. The analysis indicates that

360 the basalt fiber length exerts a significant impact on the q_p of samples, and shorter
361 fiber length of 3 mm is proved to be more effective than longer fibers of 7 mm and 11
362 mm in enhancing the triaxial shear behavior of cemented kaolinite. This finding is in
363 good agreement with that reported by Prabakar et al. [27], and the relevant
364 microstructural mechanisms will be discussed as follows.
365 In order to study the effect of σ_3 levels, the mechanical properties of BFCK samples
366 defined by triaxial tests are reported in Fig. 7, which shows the q_p evolution of
367 cement-fiber treated samples under three different σ_3. The q_p values of K6P0.2B-3
368 sample at σ_3 of 50 kPa, 100 kPa and 200 kPa are respectively 3.15 MPa, 3.71 MPa
369 and 4.52 MPa, which are evidently higher than that of other samples.
370 For cement-fiber solidified samples, the q_p has an increasing trend with growing σ_3,
371 but R_f presents differently a decreasing tendency. It is potentially because that the
372 cemented kaolinite remains relatively loose under lower σ_3 and a large number of tiny
373 pores may exist inside the samples. Owing to the augmentation in σ_3, the diminution
374 in pore size and pore volume inside kaolinite samples takes place by expulsion of free
375 water, and the biting force between basalt fibers and kaolinite particles increases,
376 enhancing the basalt fiber reinforcement and sample stiffness.

377 ## 3.3 Microstructure

378 ### 3.3.1 Micro-mechanisms related to basalt fiber inclusion

379 To understand the macroscopic behavior of basalt fiber-reinforced kaolinite, the
380 microstructural observation should be performed by SEM **tests** and the results are
381 shown in Figures 8-10. Fig. 8 (a) gives the SEM image of BFUK typical specimen
382 with basalt fiber content of 0.2 % after being subjected to UCS tests. The shape and
383 location of basalt fiber could be clearly identified, appearing inside the typical

specimen of uncemented kaolinite. In the local marked magnified area in Fig. 8 (b), it is easier to detect that the basalt fiber surface is attached by many kaolinite minerals, which is indicative of a good bonding between kaolinite particles and basalt fibers. Due to the firmly reinforced interaction between basalt fibers and kaolinite particles, they are capable of jointly bearing the external loadings [28], and the interfacial force between kaolinite particles and basalt fibers increases gradually to resist the external loading imposed on BFUK samples [29]. In this case, the surface roughness of fiber plays an important role in ameliorating the interface friction between fiber and kaolinite particles, improving the resistance to the external loading.

Fig. 8 (c) shows the SEM image of typical specimen BFCK solidified with 6 % cement plus 0.2 % basalt fiber. The surface of basalt fiber is widely attached by the hydration products (ettringite AFt and C-S-H gels) of cement and less kaolinite minerals in comparison with the SEM image presented in Fig. 8 (a). It is well known that the main hydration products **(C-S-H gels, AFt etc.)** can greatly improve the strength performance by cementing fine grains and filling pore spaces [1-8]. This helps to improve the physical bonding strength of kaolinite particles and enhance the adhesion of basalt fiber with cemented soil matrix.

Fig. 8 (d) shows the local marked magnified area as outlined in Fig. 8 (c). **It is clear that the hydration products including fine fibrillar C-S-H gels (they might grow gradually into reticulate or honeycomb-like network as reaction proceeds) and rod-like AFt crystals are wrapped tightly around cement grains and effectively restricts the relative movement between basalt fibers and cemented aggregates**

406 **(especially at cement-fibre interface). To firmly support the SEM analysis on**
407 **cement-fiber solidified soil, the EDX patterns of C-S-H gels and Aft are shown in**
408 **Figure 8 (e)-(f). The rod-like structure found at some locations in Figure 8(e)**
409 **contains calcium, silica, oxygen and significant amount of sulfur and can be**
410 **labeled as Aft, and this finding agrees well with Li et al. [30]. The gel-like**
411 **structure marked in Figure 8(f) reveals the presence of calcium, silica and oxygen**
412 **in high concentrations and could be confirmed as C-S-H gels (gelled aggregates**
413 **contained potentially Aft and fine soil), and this conclusion has a good agreement**
414 **with Alawad et al. [31].** Therefore, this contributes significantly to the solidification
415 benefit brought by the coupling effect of basalt fiber inclusion and cementitious
416 hydration products, and the strength of BFCK is reasonably much higher than that of
417 BFUK. This is the main reason why the combination of basalt fiber and cement
418 hydration seems to be more efficient and attractive in improving the strength behavior
419 than the single addition of basalt fiber or cement alone.

420 **3.3.2 Identification of fiber distribution mode and interface friction**

421 Fig. 9 shows the distribution modes of basalt fibers embedded within the BFCK
422 specimens at 200 times magnification. It is obvious that the randomly distributed
423 basalt fibers in these specimens act similarly to the plant roots, and meanwhile, the
424 high binding ability of hydration products attached on the fiber surface toughens the
425 randomly distributed fibers as well, distributing the applied stresses in a broader area
426 and inhibiting further the fissure propagation. According to the SEM micrograph in
427 Fig. 9 (a), it can be clearly seen that a few basalt fibers are tightly surrounded by

kaolinite particles within BFCK specimen with 0.1 % basalt fiber. For the SEM micrograph of BFCK with 0.2 % basalt fiber in Fig. 9 (b), the surface of basalt fiber is attached by cement hydration products and kaolinite matrix, strengthening the interfacial interaction between fiber, cement and kaolinite. Accordingly, the basalt fibers, cement hydration products and kaolinite particles contribute jointly to the formation of a stable and interconnected structure inside the specimens through the combined action of cementation, pore filling and bridging. When the samples are subjected to external loading, the bridging effect of fibers and cementation effect of hydration products can efficiently impede the further development of tension cracks and the loading-related deformation of kaolinite samples. As a result, the basalt fiber-reinforced cemented kaolinite demonstrates in Fig. 2 (b) a somewhat stronger ductile behavior. This provides a reasonable explanation for the notable change in the brittleness-ductility characteristics (i.e. stress-strain behavior) of cement-fiber reinforced kaolinite samples.

Owning to the further addition of basalt fiber, more basalt fibers per unit section can be identified in the SEM micrograph of BFCK specimen with 0.3 % basalt fiber in Fig. 9 (c), where the basalt fibers are non-uniformly distributed. This can result in a more intensified mechanical interaction between basalt fibers inside the specimens and also the potential formation of weak surface. Note that the phenomenon of fiber agglomeration may occur in the case of non-uniformly mixed matrix. As a result, the basalt fiber may slide out of the cemented kaolinite specimen when subjected to external loading and the sliding failure occurs most probably along the weak surface.

Therefore, the presumable reason for the UCS decrease of sample with 0.3 % basalt fiber is closely related to the non-uniform distribution of basalt fibers, which have also been mentioned by Ma and Gao [15] and Ahmad and Chen [32]. This may be the dominant reason why further inclusion of basalt fiber beyond its optimum amount brings about a drop in the compressive strength and shear resistance of fiber-cement solidified specimens. Hence, it can be proposed that the strength improvement of BFCK samples depends principally on three factors: (i) tensile strength of basalt fiber, (ii) surface roughness of basalt fiber and bonding behavior of cemented kaolinite and (iii) distribution and size of basalt fiber in cemented kaolinite. The cementitious hydration products of cement and reinforcement of basalt fibers create altogether a better bridging property, reinforce the interlocking of cemented aggregates and fill in pore spaces within cemented kaolinite, which without doubt leads to superior strength performance than cemented kaolinite without basalt fiber.

As presented in Fig. 10, the experimental evidence is captured to identify the interface friction between basalt fiber and kaolinite. Fig. 10 (a) shows the pullout behavior of basalt fibers, in which a scratch trace is formed on the specimen section and the failure mechanism of BFCK is revealed. When the specimen is subjected to external loading, the basalt fibers with excellent tensile strength can further prevent the extension of cracks and prolongation of fractures, until they are pulled out of kaolinite specimens. The interface friction between fiber and cemented particles, which is closely related to the surface roughness of basalt fiber, provides a strong pullout resistance to the tensile traction transformed from external loading. As shown in Fig.

472 10 (b), the scratch trace at the ends of basalt fibers can also be observed, and this may
473 be predominantly the original section formed during the fiber production process or
474 caused by the friction between basalt fibers and hard particles. In Fig. 8 and Fig. 9, it
475 is apparent that most of the basalt fibers are naturally stretched due to its excellent
476 mechanical performance and the surface has no evident deformation or scratch. This
477 is different from the phenomenon of a lot of scratches squeezed on the surface of
478 polypropylene fibers in the marked area of Fig. 10 (c), because the basalt fiber has
479 much more excellent mechanical resistance to deformation than the polypropylene
480 fiber.

481 **3.3.3 Schematic illustration of fiber-cement-kaolinite system**

482 The mechanical strength of cement-stabilized soils are greatly influenced by several
483 factors such as cement content, curing time and water to cement ratio [1,5,6,33,34],
484 which are tightly associated with a series of physic-chemical reactions including
485 cation exchange, flocculation, hydration and potential pozzolanic reactions between
486 cement and moist soils. The chemical reactions can generate new cementitious phases,
487 such as C-S-H gels and ettringite etc., as detected in SEM images, and promote the
488 structural integrity and mechanical behavior of cemented kaolinites by physical
489 bonding and pore-filling. The incorporation of basalt fiber into kaolinite matrix can
490 produce a reinforcement effect, which would affect the stiffness, failure strain and
491 compressive strength of stabilized kaolinites [11,12,25,28]. The bridging benefit of
492 basalt fiber could intensify the interfacial interaction between basalt fiber and
493 kaolinite particle, including interface cohesion and interface interaction. This can

494 effectively improve the resistance of kaolinite to deformation and limit the
495 development of micro-cracks within samples. Especially, shorter basalt fiber increases
496 the contact area and interface force between fiber and kaolinite, thereby improving the
497 net-like interconnected structure and the mechanical performance of cement-fiber
498 stabilized kaolinite.

499 According to the above-stated SEM analysis, Figure 11 summarizes the interfacial
500 mechanical behavior of kaolinite stabilized with cement-basalt fiber. It can be found
501 that the mechanical interaction between basalt fibers, **cement hydration products**
502 **(C-S-H gels, AFt etc.)** and clay particles is mainly composed by three forces
503 originating from different sources: (i) the hydration products of cement can effectively
504 bond clay particles and basalt fibers together, leading to the formation of a
505 well-interconnected and stable skeletal structure; (ii) the adhesive force is the main
506 force between basalt fibers and kaolinite particles since the kaolinite is mainly
507 composed of fine particles; and (iii) certain amount of kaolinite particles are attached
508 on the rough surface and edge of basalt fibers, which would produce the
509 non-negligible biting force and interface fiction to restrict the deformation and relative
510 movement when the samples are subjected to external loading. Especially, a small
511 amount of carbonates might unexpectedly emerge in certain cases owning to the
512 carbonation of reactive binder after exposure to CO_2 in air during the mixture
513 preparation and standard curing of samples, and the carbonation reactions and
514 corresponding products have been systematically discussed by Wang et al. [35-38].

515 # 4 Conclusions

As an eco-friendly and biologically inactive material that until now attracts very little attention, the combination of basalt fiber with cement has been proposed as an efficient and cost-effective method to treat soft clays in ground engineering. This study highlights the effect of basalt fiber inclusion on the mechanical properties and microscopic mechanisms of kaolinite through a series of UCS, TC and SEM tests. The main conclusions drawn from the obtained data are summarized as follows.

(i) The basalt fiber reinforcement combined with cement stabilization is demonstrated to be effective for the improvement in the compressive strength and shear resistance of kaolinite. However, the single presence of basalt fiber plays a minor influence on the compressive strength in comparison with the combination of basalt fiber and cement, which has the virtues of both basalt fiber-reinforced kaolinite and cement-stabilized kaolinite.

(ii) The inclusion of basalt fiber can improve the ductility behavior and post-peak strength of cemented kaolinite owing to the bridging effect. It exists an optimum basalt fiber content of 0.2 % where the UCS reaches its peak, and higher or lower content of basalt fiber causes strength degradation rather than an improvement.

(iii) The peak deviatoric stress defined by triaxial tests have an increasing trend until an optimum basalt fiber content of 0.4 %, after which further increase in fiber content reduces the reinforcement effect due to its non-uniform distribution within samples. Short fiber length of 3 mm is proved more effective in improving the peak deviatoric stress of cemented kaolinite than longer fiber of 7 mm and 11 mm. The elevated confining pressure results in a continuous improvement in the peak deviatoric stress.

(iv) The interfacial mechanical interaction between kaolinite, cement hydration product and basalt fiber contributes to the formation of a well-interconnected skeletal structure by the combination of fiber reinforcement and cement stabilization. This is the main reason why the inclusion of randomly distributed basalt fiber can greatly improve the mechanical performance of cemented kaolinite.

Acknowledgment

This work was supported by the National Natural Science Foundation of China (Grant no. 51879202, no. 51609180).

References

[1] T. Deng, Y. Deng, X. Yue, Y. Cui, Deterioration of marine soft clay at east China solidified by cement-metakaolin composite, Environ. Geotech., (2019) https://doi.org/10.1680/jenge.18.00202.

[2] D. Wang, R. Zentar, N. E. Abriak, Durability and swelling of solidified/stabilized dredged marine soils with class F fly ash, cement and lime, J. Mater. Civil Eng. 30(3) (2018) 04018013.

[3] D. Wang, R. Wang, M. Benzerzour, H. Wang, N.E. Abriak, Comparison between reactive MgO- and Na_2SO_4-activated low-calcium fly ash solidified soils dredged from East Lake, China, Mar. Georesour. Geotec. (2019) DOI: 10.1080/1064119X.2019.1648616.

[4] D. Wang, N. E. Abriak, R. Zentar, One-dimensional consolidation of lime-treated

560 dredged harbour sediments, Eur. J. Environ. Civil En. 19(2) (2015) 199-218.
561 [5] D. Wang, L. Korkiala-Tanttu, On the normalized behaviour of naturally and
562 artificially structured clays, Eng. Geol. 214 (2016) 20-28.
563 [6] D. Wang, N. E. Abriak, R. Zentar, Temperature-accelerated strength development
564 in stabilised marine soils as road construction materials, J. Mater. Civil Eng. 2017,
565 29(5): 04016281.
566 [7] B. K. Dahal, J. J. Zheng, R. J. Zhang, D. B. Song, Enhancing the mechanical
567 properties of marine clay using cement solidification, Mar. Georesour. Geotec. 37(6)
568 (2019) 755-764.
569 [8] L. Liu, A. Zhou, Y. Deng, Y. Cui, Z. Yu, C. Yu, Strength performance of
570 cement/slag-based stabilized soft clays, Constr. Build. Mater. 211 (2019) 909-918.
571 [9] P. Jamsawang, H. Poorahong, N. Yoobanpot, S. Songpiriyakij, P. Jongpradist,
572 Improvement of soft clay with cement and bagasse ash waste, Constr. Build. Mater.
573 154 (2017) 61-71.
574 [10] X. Kang, G. C. Kang, K. Chang, L. Ge, Chemically stabilized soft clays for
575 road-base construction, J. Mater. Civil Eng. 27(7) (2015) 04014199.
576 [11] Y. X. Wang, P. P. Guo, X. Li, H. Lin, Behavior of fiber-reinforced and
577 lime-stabilized clayey soil in triaxial tests, Appl. Sci.-Basel 9(5) (2019) 900.
578 [12] C. S. Tang, D. Y. Wang, Y. J. Cui, B. Shi, J. Li, Tensile strength of
579 fiber-reinforced soil, J. Mater. Civil Eng. 28(7) (2016) 04016031.
580 [13] A. Ammar, S. Najjar, S. Sadek, Mechanics of the interface interaction between
581 hemp fibers and compacted clay, Int. J. Geomech. 19(4) (2019) 04019015.

582 [14] Y. Wang, P. Guo, F. Dai, X. Li, Y. Zhao, Y. Liu, Behavior and modeling of
583 fiber-reinforced clay under triaxial compression by combining the superposition
584 method with the energy-based homogenization technique, Int. J. Geomech. 18(12)
585 (2018) 04018172.
586 [15] Q. Ma, C. Gao, Effect of basalt fiber on the dynamic mechanical properties of
587 cement-soil in SHPB test, J. Mater. Civil Eng. 30(8) (2018) 04018185.
588 [16] M. E. Orakoglu, J. K. Liu, F. J. Niu, Dynamic behavior of fiber-reinforced soil
589 under freeze-thaw cycles, Soil. Dyn. Earthq. Eng. 101 (2017) 269-284.
590 [17] P. Sharma, An introduction to basalt rock fiber and comparative analysis of
591 engineering properties of BRF and other natural composites, International Journal for
592 Research in Applied Science & Engineering Technology 4(I) (2016) 141-147.
593 [18] H. Jamshaid, R. Mishra, A green material from rock: basalt fiber - a review, J.
594 Text. I. 107(7) (2016) 923-937.
595 [19] C. Buratti, E. Moretti, E. Belloni, F. Agosti, Thermal and acoustic performance
596 evaluation of new basalt fiber insulation panels for buildings, Energy Procedia 78
597 (2015) 303-308.
598 [20] A. G. Novitskii, High-temperature heat-insulating materials based on fibers from
599 basalt-type rock materials, Refract. Ind. Ceram. 45(2) (2004) 144-146.
600 [21] E. Moretti, E. Belloni, F. Agosti, Innovative mineral fiber insulation panels for
601 buildings: Thermal and acoustic characterization, Appl. Energ. 169 (2016) 421-432.
602 [22] Y. V. Lipatov, S. I. Gutnikov, M. S. Manylov, E. S. Zhukovskaya, B. I. Lazoryak,
603 High alkali-resistant basalt fiber for reinforcing concrete, Mater. Design 73 (2015)

60-66.

[23] A. B. Kizilkanat, N. Kabay, V. Akyüncü, S. Chowdhury, A. H. Akça, Mechanical properties and fracture behavior of basalt and glass fiber reinforced concrete: An experimental study, Constr. Build. Mater. 100 (2015) 218-224.

[24] JTG E40-2007, Test Method of Soils for Highway Engineering, Ministry of Transport of PRC., Beijing: China Communications Press, 2007.

[25] C. Tang, B. Shi, W. Gao, F. Chen, Y. Cai, Strength and mechanical behavior of short polypropylene fiber reinforced and cement stabilized clayey soil, Geotext. Geomembranes 25(3) (2007) 194-202.

[26] D. Wang, N. E. Abriak, R. Zentar, W. Y. Xu, Solidification/stabilization of dredged marine sediments for road construction, Environ. Technol. 33(1) (2012) 95-101.

[27] J. Prabakar, R. S. Sridhar, Effect of random inclusion of sisal fibre on strength behaviour of soil, Constr. Build. Mater. 16(2) (2002) 123-131.

[28] C. S. Tang, B. Shi, L. Z. Zhao, Interfacial shear strength of fiber reinforced soil, Geotext. Geomembranes 28(1) (2010) 54-62.

[29] N. Cristelo, V. M. Cunha, M. Dias, A. T. Gomes, T. Miranda, N. Araújo, Influence of discrete fibre reinforcement on the uniaxial compression response and seismic wave velocity of a cement-stabilised sandy-clay, Geotext. Geomembranes 43(1) (2015) 1-13.

[30] H. Li, X. Guan, X. Zhang, P. Ge, X. Hu, D. Zou, Influence of superfine ettringite on the properties of sulphoaluminate cement-based grouting materials, Constr. Build.

626 Mater. 166 (2018) 723-731.
627 [31] O. A. Alawad, A. Alhozaimy, M. S. Jaafar, A. Al-Negheimish, F. N. A. Aziz,
628 Microstructure analyses of autoclaved ground dune sand-Portland cement paste,
629 Constr. Build. Mater. 65 (2014) 14-19.
630 [32] M. R. Ahmad, B. Chen, Effect of silica fume and basalt fiber on the mechanical
631 properties and microstructure of magnesium phosphate cement (MPC) mortar, Constr.
632 Build. Mater. 190 (2018) 466-478.
633 [33] D. Wang, L. Korkiala-Tanttu, 1-D compressibility behaviour of cement-lime
634 stabilized soft clays, Eur. J. Environ. Civ. En. (2019) DOI
635 10.1080/14680629.2018.1439400.
636 [34] D. Wang, X. Gao, R. Wang, S. Larsson, M. Benzerzour, Elevated curing
637 temperature-associated strength and mechanisms of reactive MgO-activated industrial
638 by-products solidified soils, Mar. Georesour. Geotec. (2019) DOI:
639 10.1080/1064119X.2019.1610817.
640 [35] D. Wang, J. Zhu, F. He, Quantification and micro-mechanisms of CO_2
641 sequestration in magnesia-lime-fly ash/slag solidified soils, Int. J. Greenh. Gas Con.
642 91 (2019) 102827.
643 [36] D. Wang, J. Zhu, F. He, CO_2 carbonation-induced improvement in strength and
644 microstructure of reactive MgO-CaO-fly ash-solidified soils, Constr. Build. Mater.
645 229 (2019) 116914.
646 [37] D. Wang, J. Xiao, F. He, Y. Zhou, Durability evolution and associated
647 micro-mechanisms of carbonated reactive MgO-fly ash solidified sludge from East

Lake, China, Constr. Build. Mater. 208 (2019) 1-12.

[38] D. Wang, J. Xiao, X. Gao, Strength gain and microstructure of carbonated reactive MgO-fly ash so-lidified sludge from East Lake, China, Eng. Geol. 251 (2019) 37-47.

Figures

Fig. 1 Basalt fibers used in this study

(a) Dispersed 3-mm length fiber (b) Dispersed 7-mm length fiber

(c) Dispersed 11-mm length fiber (d) Clustered 3-mm length fiber

(e) Clustered 7-mm length fiber (f) Clustered 11-mm length fiber

Fig. 2 Stress-strain analysis of kaolinite samples under varying basalt fiber contents at 28 d

(a) BFUK (b) BFCK

Fig. 3 Compressive strength of kaolinite samples under varying basalt fiber contents

(a) BFUK (b) BFCK

Fig. 4 Typical deviatoric stress-strain relationships by triaxial tests on BFCK samples

(a) At varying basalt fiber contents and confining pressure of 100 kPa

(b) At varying basalt fiber lengths and confining pressure of 100 kPa

(c) At varying confining pressures for samples K6P0.2B-11 and K6P0B

Fig. 5 Variation of deviatoric stress at peak state and peak stress ratio with varying basalt fiber contents

(a) peak deviatoric stress (b) peak stress ratio

Fig. 6 Variation of peak deviatoric stress and peak stress ratio with varying basalt fiber lengths at 0.2 % basalt fiber

(a) peak deviatoric stress (b) peak stress ratio

Fig. 7 Variation of peak deviatoric stress and peak stress ratio at varying confining

pressures

(a) peak deviatoric stress (b) peak stress ratio

Fig. 8 SEM images and EDX patterns of typical specimens

(a) BFUK with 0.2 % basalt fiber (×2000)

(b) local marked magnified area of (a) (×5000)

(c) BFCK with 0.2 % basalt fiber (×2000)

(d) local marked magnified area of (c) (×5000)

(e) EDX pattern of AFt

(f) EDX pattern of C-S-H

Fig. 9 Distribution of basalt fibers in BFCK

(a) 0.1 % basalt fiber (×200) (b) 0.2 % basalt fiber (×200)

(c) 0.3 % basalt fiber (×200)

Fig. 10 Experimental evidence of friction between fiber and kaolinite

(a) pullout of basalt fibers forms a scratch on the kaolinite section

(b) a scratch at the end of basalt fiber

(c) lots of scratches on the polypropylene fiber surface (from Tang et al. [29])

Fig. 11 Sketch of interfacial mechanical behavior between kaolinite particles, cement hydration products and basalt fibers

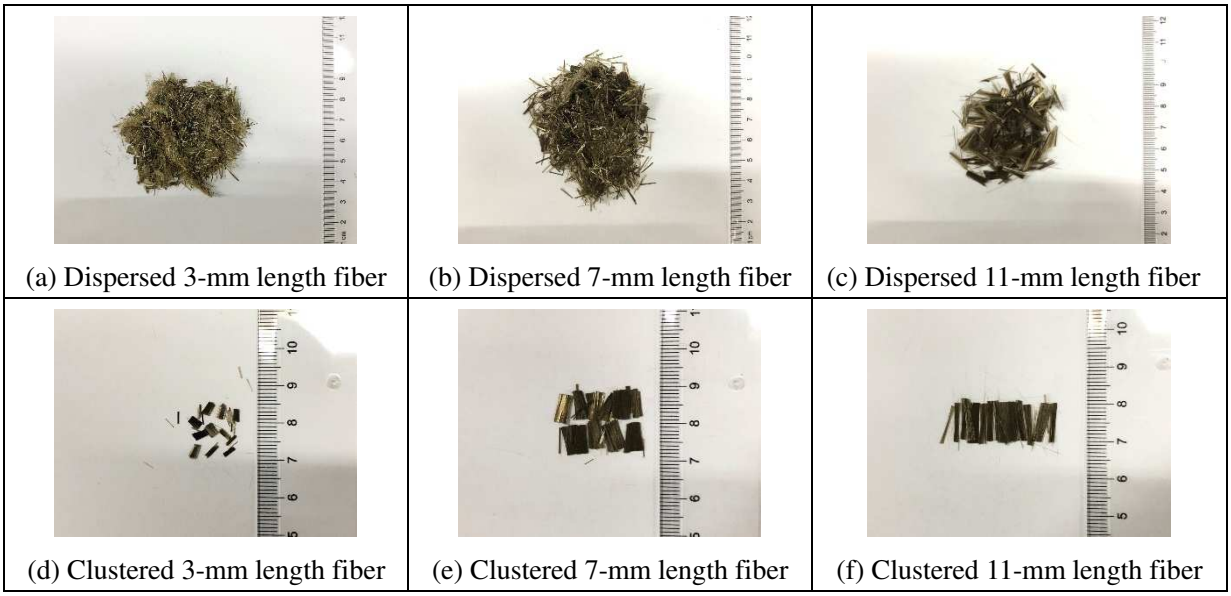

(a) Dispersed 3-mm length fiber | (b) Dispersed 7-mm length fiber | (c) Dispersed 11-mm length fiber

(d) Clustered 3-mm length fiber | (e) Clustered 7-mm length fiber | (f) Clustered 11-mm length fiber

Fig. 1 Basalt fibers used in this study

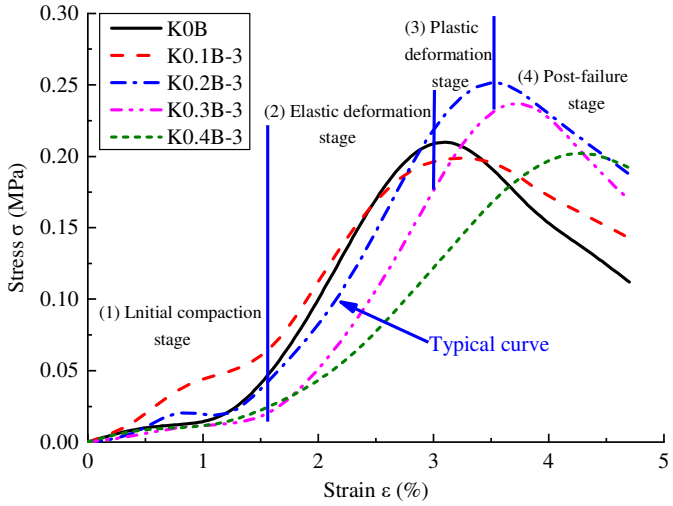

(a) BFUK

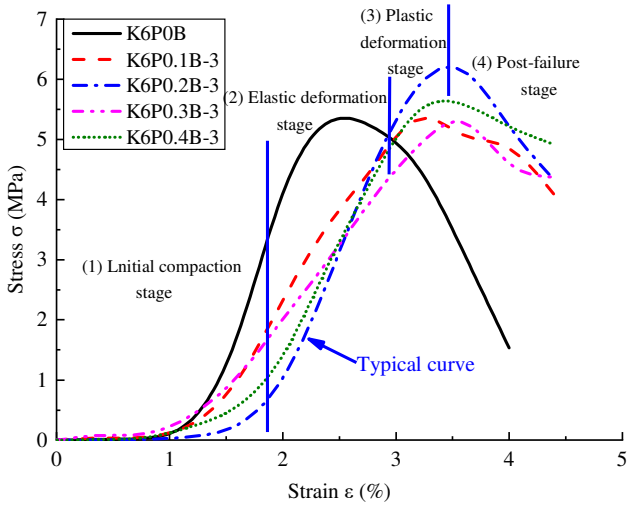

(b) BFCK

Fig. 2 Stress-strain analysis of kaolinite samples under varying basalt fiber contents at 28 d

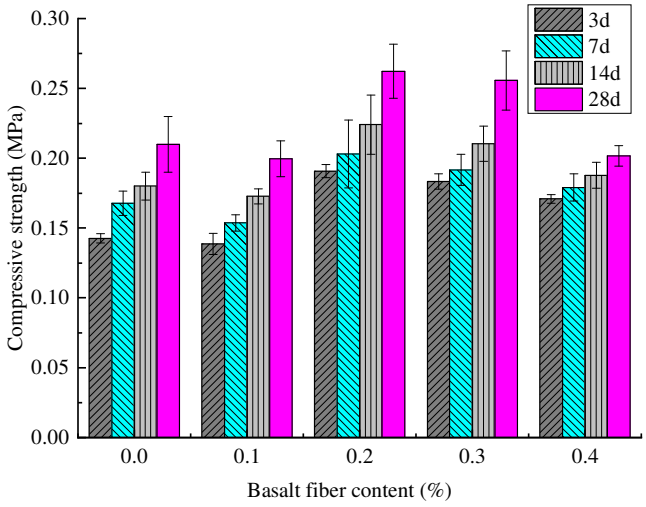

(a) BFUK

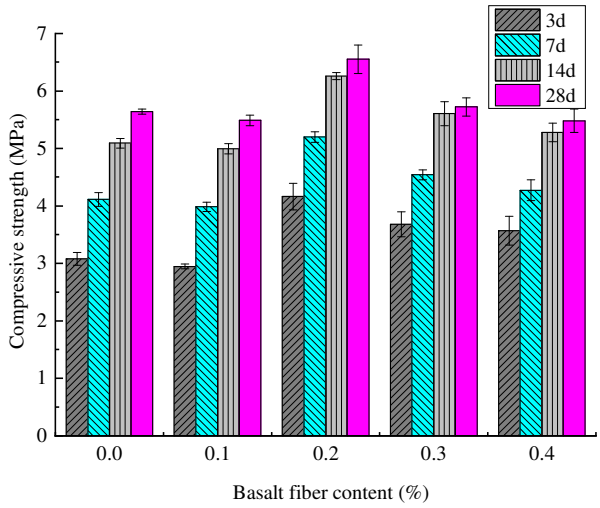

(b) BFCK

Fig. 3 Compressive strength of kaolinite samples under varying basalt fiber contents

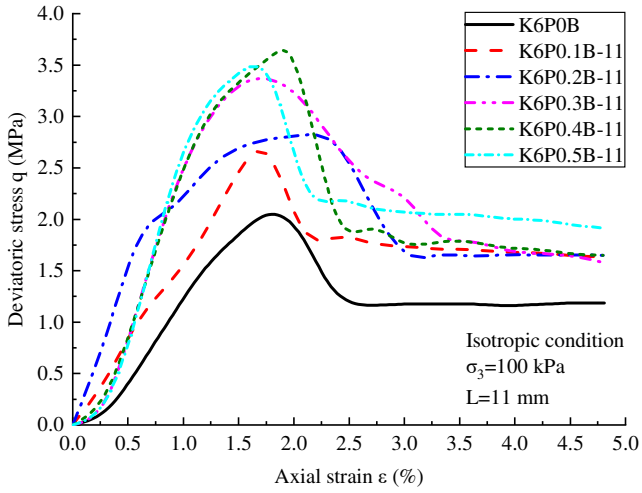

(a) At varying basalt fiber contents and confining pressure of 100 kPa

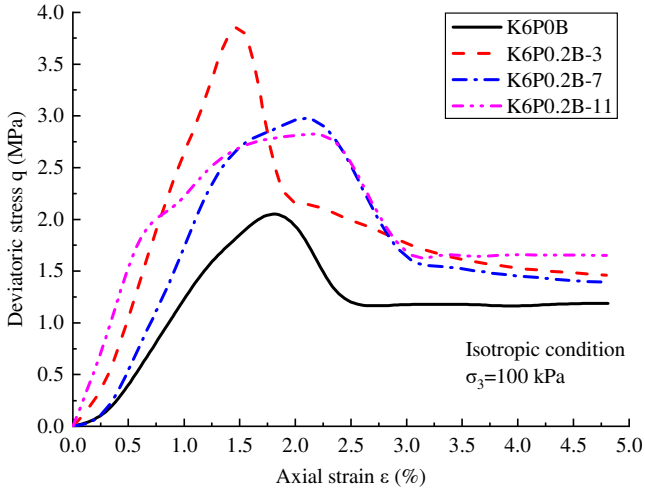

(b) At varying basalt fiber lengths and confining pressure of 100 kPa

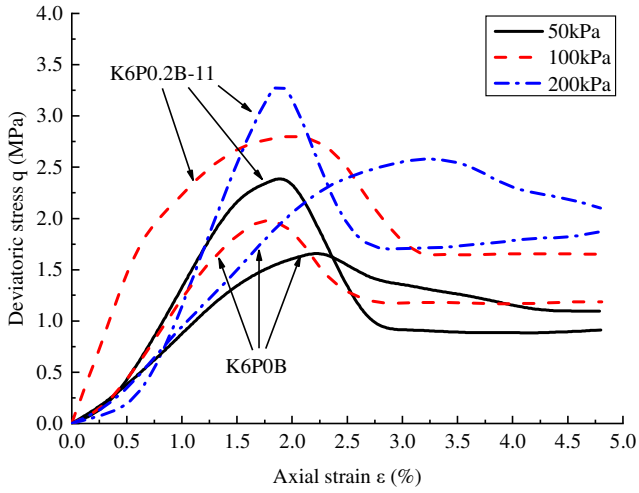

(c) At varying confining pressures for samples K6P0.2B-11 and K6P0B

Fig. 4 Typical deviatoric stress-strain relationships by triaxial tests on BFCK samples

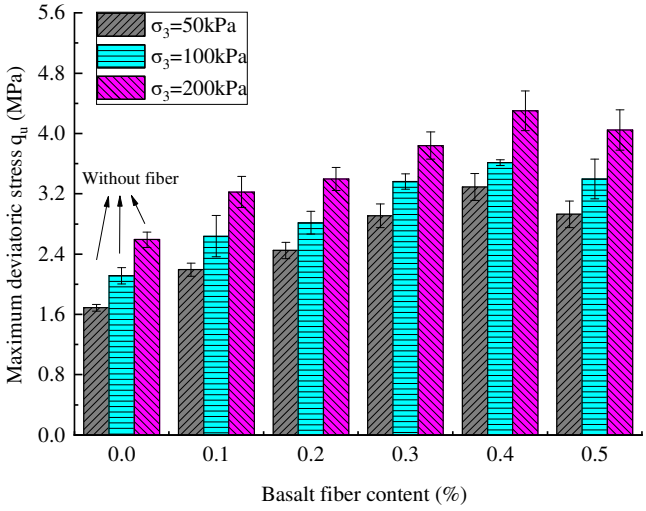

(a) Peak deviatoric stress

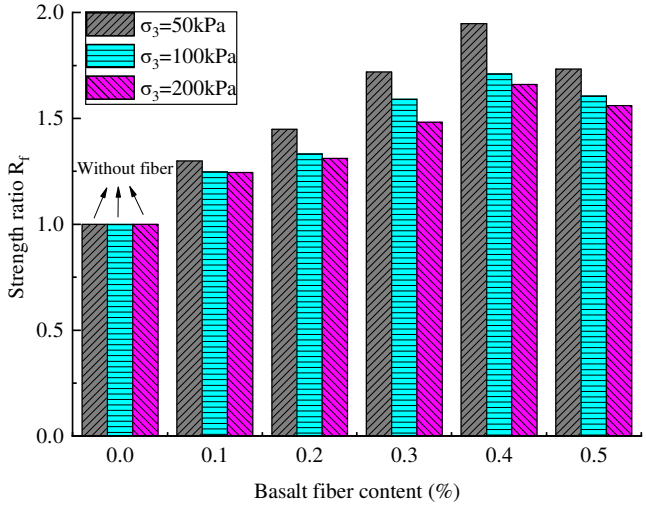

(b) Peak stress ratio

Fig. 5 Variation of deviatoric stress at peak state and peak stress ratio with varying basalt fiber contents

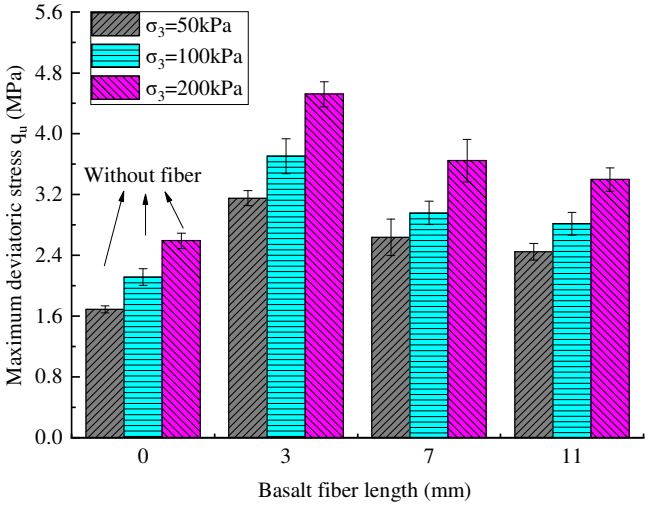

(a) Peak deviatoric stress

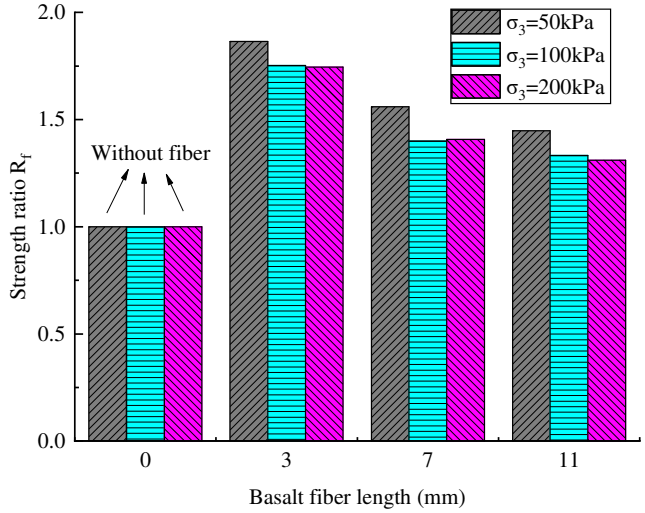

(b) Peak stress ratio

Fig. 6 Variation of peak deviatoric stress and peak stress ratio with varying basalt fiber lengths at 0.2 % basalt fiber

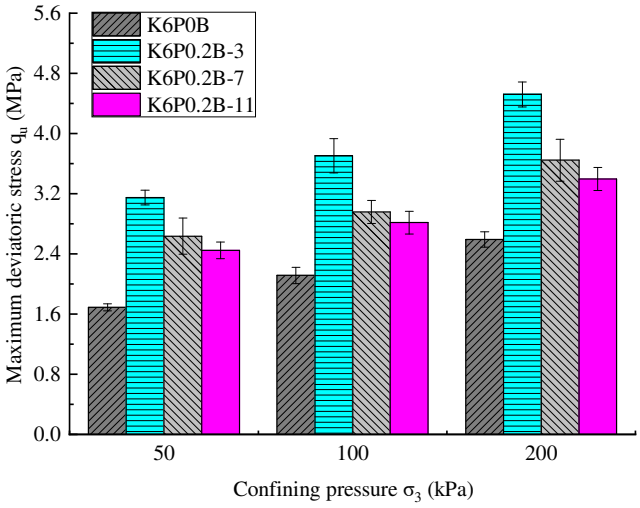

(a) Peak deviatoric stress

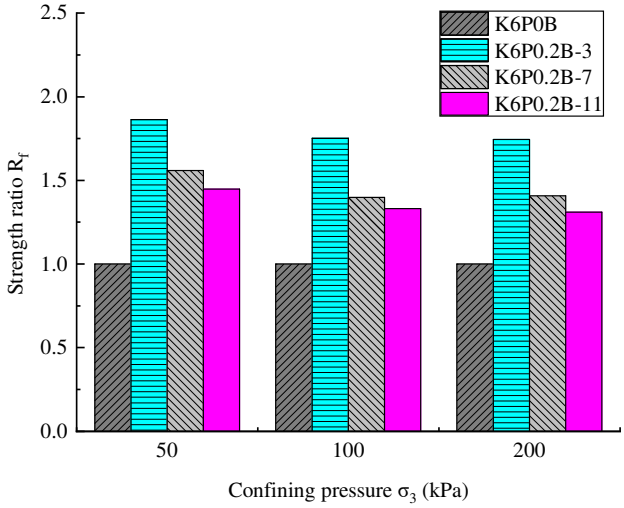

(b) Peak stress ratio

Fig. 7 Variation of peak deviatoric stress and peak stress ratio at varying confining pressures

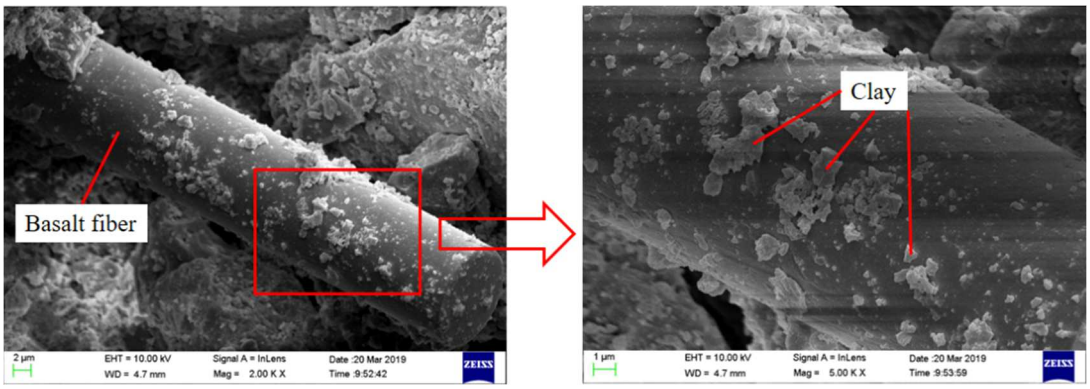

(a) BFUK with 0.2 % basalt fiber (×2000) (b) local marked magnified area of (a) (×5000)

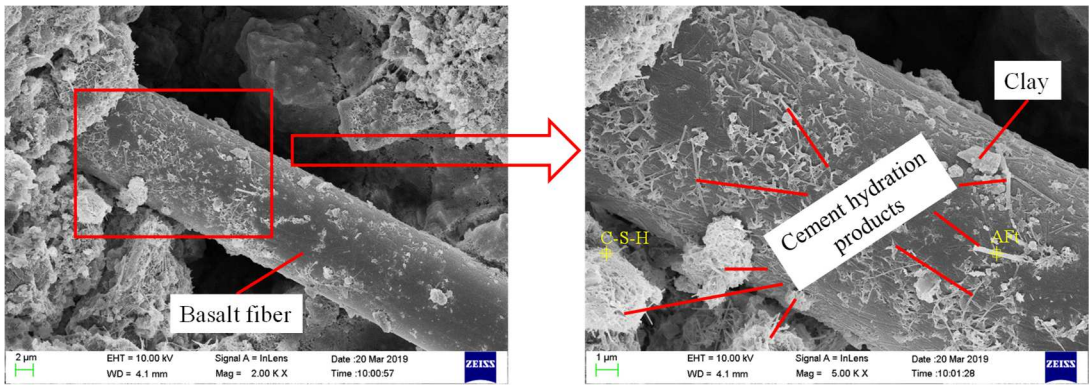

(c) BFCK with 0.2 % basalt fiber (×2000) (d) local marked magnified area of (c) (×5000)

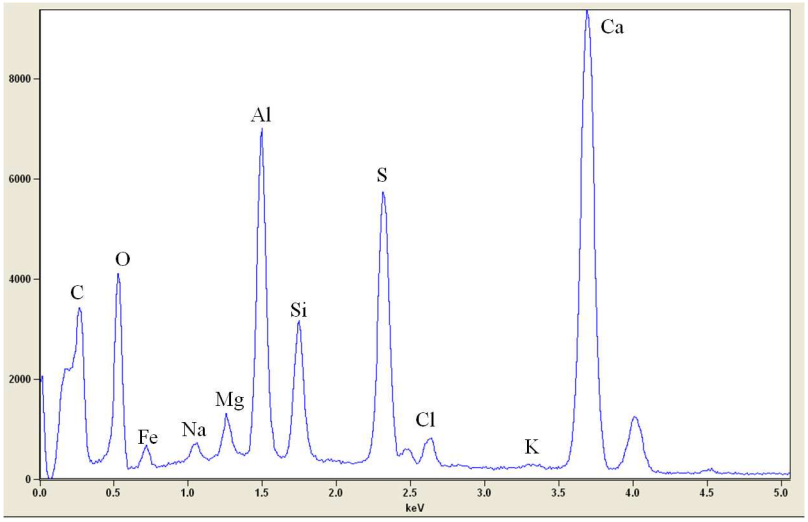

(e) EDX pattern of Aft

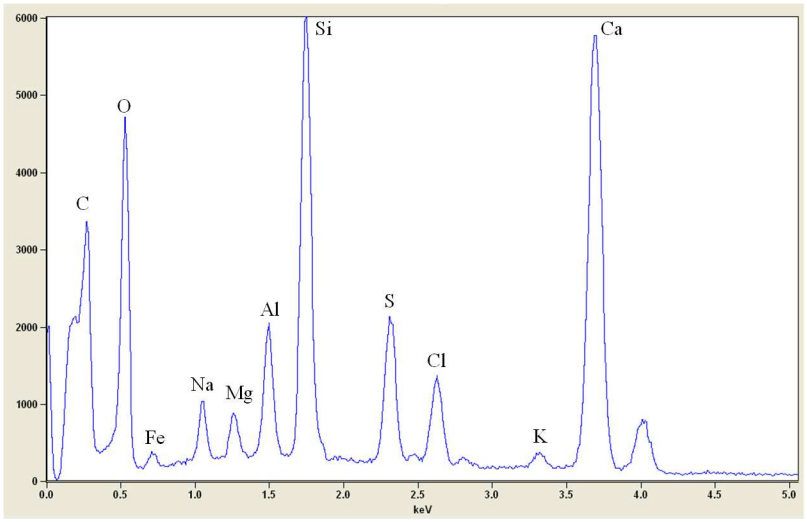

(f) EDX pattern of C-S-H

Fig. 8 SEM images and EDX patterns of typical specimens

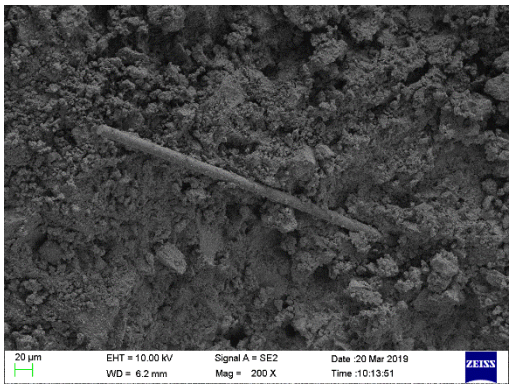

(a) 0.1 % basalt fiber (×200)

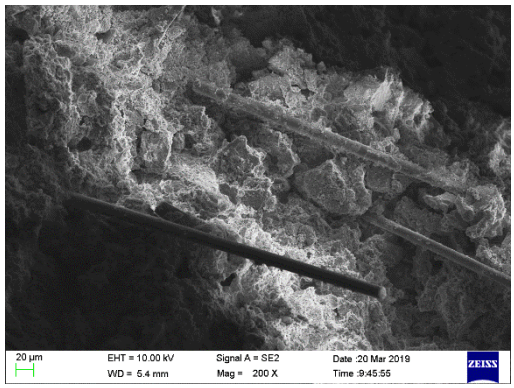

(b) 0.2 % basalt fiber (×200)

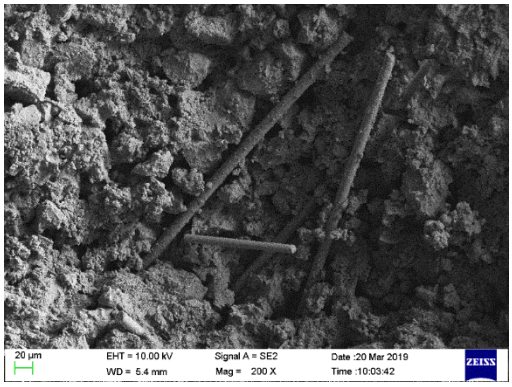

(c) 0.3 % basalt fiber (×200)

Fig. 9 Distribution of basalt fibers in BFCK

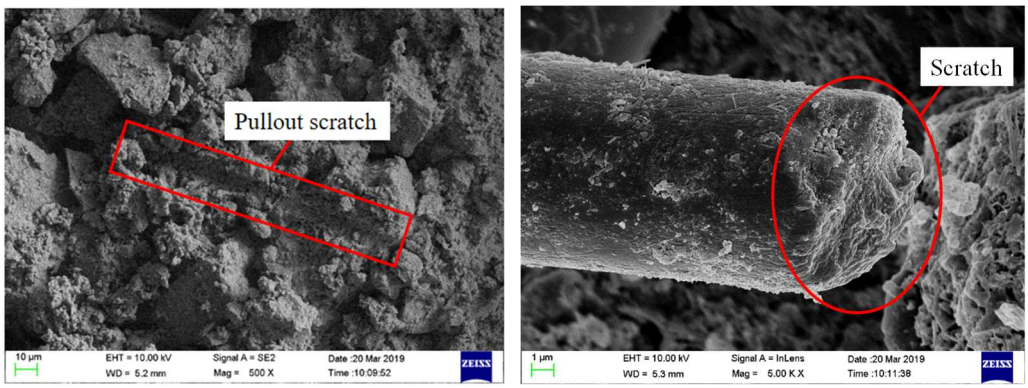

(a) pullout of basalt fibers forms a scratch on the kaolinite section (b) a scratch at the end of basalt fiber

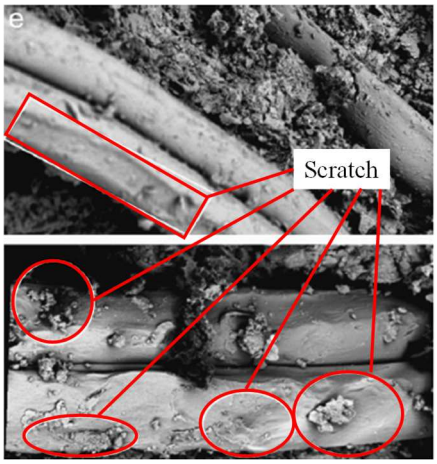

(c) lots of scratches on the polypropylene fiber surface (from Tang et al. [25])

Fig. 10 Experimental evidence of friction between fiber and kaolinite

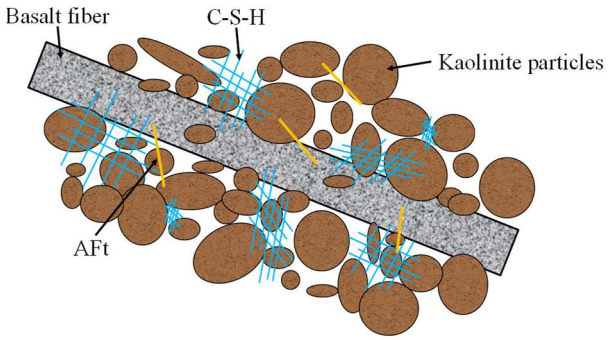

Fig. 11 Sketch of interfacial mechanical behavior between kaolinite particles, cement hydration products and basalt fibers

Tables

Table 1 Basic physical characteristics of kaolinite

Parameters	Values
Initial water content (%)	0.17
Specific gravity	2.75
Liquid limit (%)	31.0
Plastic limit (%)	20.1
Plasticity index (%)	10.9
Optimum water content (%)	22.4
Maximum dry density (g/cm^3)	1.62

Table 2 Chemical compositions of ordinary Portland cement

Chemical composition	Content by mass (%)
CaO	62.4
SiO_2	22.6
Al_2O_3	5.7
Fe_2O_3	4.3
MgO	0.8
SO_3	1.1
Other oxides	3.1

Table 3 Technical specifications of employed basalt fiber

Parameter	Value
Fiber type	Monofilament
Density (g/cm^3)	2.63
Diameter (μm)	7-15
Tensile strength (MPa)	3000-4800
Modulus of elasticity (GPa)	91-110
Melting point (°C)	1050
Acid and alkali resistance	Excellent

Table 4 Mix formulations (wt%) for UCS and CU triaxial tests

Types of tests	Group	Mixture ID	Content (% by weight)			Length of basalt fiber (mm)	Curing time (d)
			Kaolinite	Cement	Basalt fiber		
UCS test	1	K0B	100	0	0	—	3, 7, 14, 28
		K0.1B	99.9	0	0.1	11	3, 7, 14, 28
		K0.2B	99.8	0	0.2	11	3, 7, 14, 28
		K0.3B	99.7	0	0.3	11	3, 7, 14, 28
		K0.4B	99.6	0	0.4	11	3, 7, 14, 28
	2	K6P0B	94	6	0	—	3, 7, 14, 28
		K6P0.1B	93.9	6	0.1	11	3, 7, 14, 28
		K6P0.2B	93.8	6	0.2	11	3, 7, 14, 28
		K6P0.3B	93.7	6	0.3	11	3, 7, 14, 28
		K6P0.4B	93.6	6	0.4	11	3, 7, 14, 28
CU TC test	3	K6P0B	94	6	0	—	7
		K6P0.1B	93.9	6	0.1	11	7
		K6P0.2B	93.8	6	0.2	11	7
		K6P0.3B	93.7	6	0.3	11	7
		K6P0.4B	93.6	6	0.4	11	7
		K6P0.5B	93.5	6	0.5	11	7
	4	K6P0.2B-3	93.8	6	0.2	3	7
		K6P0.2B-7	93.8	6	0.2	7	7
		K6P0.2B-11	93.8	6	0.2	11	7